El Cezeri
Journal of Science and Engineering
ISSN: 2148-3736

Research Article

Enhanced Histopathological Image Classification through the fusion of Thepade Sorted Block Truncation Code and Otsu Binarization features

Sudeep D. Thepade[1a], Ashwin Acharya[1b],
[1] Department of Computer Engineering, Pimpri Chinchwad College of Engineering, Pune, India
sudeepthepade@gmail.com

DOI : 10.31202/ecjse.1380112
Received: 23.10.2023 Accepted: 20.02.2024
How to cite this article:
Sudeep D. Thepade, Ashwin Acharya, " Enhanced Histopathological Image Classification through the fusion of Thepade Sorted Block Truncation Code and Otsu Binarization features", El-Cezeri Journal of Science and Engineering, Vol: 11, Iss:2, (2024), pp.(175-185).
ORCID: [a]0009-0007-9520-9972; [b]0000-0001-7809-4148.

Abstract : Histopathology is the branch of pathology that investigates the structure of cells and tissues of organisms at a microscopic level. Histopathological images are crucial in the decision-making process for effective therapies, determining the health of a particular biological structure and identifying diseases like cancer. With machine learning models, it may be feasible to increase the accuracy of medical data, decrease patient rate variations, and cut costs associated with medical care. Most medical scientists are drawn to such new technologies of predictive models in chronic disease forecasting. A novel approach for more accurate classification of histopathological images is proposed in this paper. The technique involves fusing the features extracted from two methods, namely Otsu's binarization and Thepade Sorted Block Truncation Code, to achieve improved results. The KIMIA Path960 dataset comprising 960 images is utilized for experimental validation with performance indicators like accuracy, specificity, and sensitivity. Ensembles of Simple Logistics, Multilayer Perceptron, Logistics Model Tree, as well as Simple Logistics, Random Forest, and Logistic Model Tree classifiers, demonstrated superior performance for the fusion of Thepade Sorted Block Truncation Code 7-ary and Otsu features, achieving an accuracy of 97.39 percent in a 10-fold cross-validation scenario.

Keywords : Histopathology, Thepade SBTC, Feature Fusion, Ensembles.

1 Introduction

According to current records, millions have died of diseases like cancer. The probability of receiving appropriate care and achieving favourable survival rates is markedly increased through early diagnosis. However, this diagnostic procedure is characterized by its protracted nature frequently engenders professional discord among pathologists. Several studies have raised concerns about the global shortage of medical professionals needed to handle the rising number of cancer patients. With cancer cases skyrocketing and a global shortfall of expert medical practitioners, machine learning can play a significant role. Machine learning (ML) algorithms can be trained to discern complex data trends, potentially revolutionizing diagnostic processes. A range of conventional ML algorithms has been applied to this problem, with varying degrees of success.

Though techniques such as X-rays and MRIs were used to diagnose cancer, biopsy remains the primary method for cancer diagnosis. Standard biopsy methods include surgical, vacuum-assisted, fine-needle aspiration, Core needle, and image-guided biopsy. The methodology involves a series of sequential steps, starting with collecting tissue or cell samples, then placing them onto a microscope slide, and concluding with applying a stain to facilitate visual differentiation. Subsequently, a diagnosis is established based on the examination of histopathological images with the knowledge of professionals. With Machine learning, this problem can be resolved. The classification of histopathological images using machine learning typically involves three key stages: classification, feature reduction, and feature extraction. A multitude of unique characteristics can be extracted from digital images, which is essential for precise categorization. The scientific literature has proposed numerous techniques for feature extraction, which are subsequently utilized for training and evaluating various machine learning algorithms. The paper presents an innovative approach to improve the classification performance of histopathological images by integrating features obtained from Otsu's binarization and Thepade SBTC methods.

Listed below are the key contributions of the presented work

- Ensemble: A methodology involving amalgamating multiple base models to form a unified predictive model that aims to optimize predictive performance.

- Feature Fusion: The method proposed uses a feature fusion of Otsu thresholding and Thepade SBTC(TSBTC) global features.
- Experimented Evaluation on the images of KIMIA Dataset: Experimentations are performed on KIMIA PATH960, which consists of images of epithelial, connective tissue and muscle.

2 Experimental Methods

2.1 Related Works

Studies on histopathological image classification have employed various techniques, including analyzing image spatial structure, classification through segmentation, and using global and window-based features. Deep feature-based classification has become increasingly popular in recent years. However, deep learning techniques necessitate intensive training and access to a balanced and extensive dataset.

Meghana et al.[1] conducted a comparative study to assess the effectiveness of different feature extraction techniques for histopathological image classification in the KIMIA Path960 dataset. The dataset consisted of 960 histopathological images belonging to 20 unique classes. The study compared the performance of bag-of-visual words (BoVW), deep features and local binary patterns (LBP) and found that LBP had an accuracy of 90.62%, deep features achieved 94.72% accuracy, and BoVW produced the highest accuracy of 96.50%. These findings highlight the superiority of BoVW over other feature extraction techniques when classifying the KIMIA Path960 dataset. This study enhances our understanding of how feature extraction affects histopathological image classification performance. In a study by Taha et al.[2], features were extracted using a pre-trained deep network, histogram of gradients and LBP from the KIMIA Path960 dataset. The extracted features were classified using standard image classification methods like artificial neural networks, decision trees and support vector machines. The findings showed that SVM yielded the highest accuracy among the three techniques at 90.52% when features were extracted using LBP. Conversely, when deep features were utilized for feature extraction, the accuracy was recorded at 81.14%. However, the results obtained using HOG were unsatisfactory.

The study by Ganguly et al. [3] investigates the influence of optimization algorithms on the accuracy of deep learning models applied to histopathological images. Two models, a pre-trained Resnet50 and a five-layer CNN, were utilized. The performance of three optimization algorithms, namely Radam, AdamW, and AdaMax, was evaluated on the KIMIA Path960 and NIA-curated lymphoma images dataset. Utilizing AdamW optimization algorithm with KIMIA Path960 dataset resulted in an accuracy of 99.9%, according to the study's findings. A slightly lower accuracy of 98.13% was achieved when the same approach was applied to the dataset of lymphoma images. The study highlights the significance of considering the optimization algorithm in conjunction with network architecture. The findings suggest that selecting the most appropriate optimization algorithm is critical in achieving optimal results in classifying histopathological images.

Anish et al.[4] utilized a pre-trained CNN for the classification of histopathological images on the KIMIA Path 960 dataset. The study aimed to explore various combinations between MobileNetV2 and GLCM (Gray-Level Co-occurrence Matrix) for histopathological image classification. The study revealed that combining the Mean of Sorted Gray Values and GLCM performed better than the other methods, with an AUC (Area Under the Curve) score of 0.999. Furthermore, the approach exhibited impressive results concerning F1 score (0.951), Precision (0.951), and Recall (0.951), emphasizing the potential of this method for improving diagnostic tools for cancer detection.

In a study by Rania et al. [5], the authors utilized the HOG feature extractor to computationally derive features from histopathological images, explicitly focusing on identifying invasive ductal carcinoma. A random subset of images, specifically 100, 200, 400, 1000, and 2000, was chosen from the histopathology dataset. These extracted statistical features were then utilized to train a range of ML algorithms. The study's primary objective was to discern between cancerous and noncancerous growth depicted in the histopathology images. The algorithms' performance was evaluated using various assessment metrics, such as AUC, F1 Score, precision, sensitivity, and accuracy. Notably, the algorithms demonstrated optimal performance when the number of images was restricted to 100, while their effectiveness diminished with a more significant number of images.

Irum et al. [6] proposed Pa-DBN-BC, a patch-based deep-learning method for histopathological image classification in breast cancer diagnosis. The method employs a Deep Belief Network (DBN) and utilizes logistic regression for image classification. The method proposed achieved an accuracy of 86%, outperforming previous deep learning methods. The authors attribute this superior performance to the ability of the method to automatically learn the best features, which sets it apart from traditional classification methods. BCHisto-Net was proposed to classify breast histopathological images at a hundred times magnification by Rashmi et al.[7] The proposed system classified breast histopathological images based on global and local features. The features were combined by a proposed feature aggregation branch, which was used to classify 100 images. The effectiveness of integrating the global and local features was observed in the paper as it accomplished an overall accuracy of 89% and 95% on the BreakHis and KMC datasets, respectively. Table 1 gives a gist of all the related work.

Despite the application of diverse techniques for histopathological image analysis in previous works, such as the examination of spatial structure, classification through segmentation, and the utilization of global and window-based features, feature fusion

Table 1: Related Works - Summary

Authors	Year of Publication	Dataset	Methodology	Advantage	Limitation
Meghana et al. [1]	2017	KIMIA Path960	LBP, Deep Features, BoVW	The automatic extraction of features is performed by Deep learning after the completion of data training	Deep Features need extensive training to achieve high accuracy.
Taha et al. [2]	2018	KIMIA Path960	Classification using SVM, Decision Tree and ANN on LBP, HOG and deep features	LBP offers significant advantages in discrimination and computational efficiency	HOG yielded unsatisfactory results due to model underperformance.
Ganguly et al. [3]	2020	KIMIA Path960, NIA dataset of lymphoma images	Pretrained Resnet50 model customized with several optimization algorithms, layered CNN	The model's extensive 23+ million trainable parameters enhance its efficacy in image recognition	Training Residual Neural Networks (ResNet) is time and resource-intensive.
Anish et al. [4]	2021	KIMIA Path960	Neural Networks + Gray-Level Co-Occurrence Matrix + Mean of sorted grey values	It exhibits a higher capacity to execute intricate tasks than other algorithms	It demands a substantial volume of data and entails significant computational costs.
Rania et al. [5]	2022	IDC subtype of breast cancer images	Statistical features extracted using HOG features extractor	The proposed method is easy to set up and operate	Performance of the model decreases when the number of images increases.
Rashmi et al. [7]	2021	BreakHis and KMC dataset	CNN-based architecture called BCHisto-Net	Global and local features extracted were combined by a feature aggregation branch	Relatively new; hence, not much research has been done on this method.

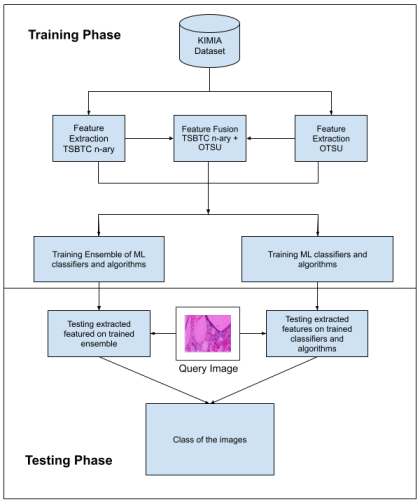

Figure 1: Block Diagram of the Proposed System

or combining both local and global features has yet to be explored extensively. Additionally, considering ensemble classifiers rather than individual ones has not been thoroughly investigated.

2.2 Proposed System

The method proposed for classifying Histopathological images consists of a training and Testing phase. Figure **??** gives an overview of the same. The extraction of image features during the training phase involves the utilization of Thepade SBTC n-ary and Otsu thresholding algorithms. Also, a fusion of extracted features from Thepade SBTC and Otsu thresholding is considered. Individual ML algorithms and classifiers and the ensemble of several classifiers and algorithms are then trained with the extracted features.

The trained classifiers and algorithms are then used to test the extracted features from the query image. The image class is identified, and the correctness accuracy is calculated. Other performance metrics, like Specificity, Sensitivity, True Positive

Rate (TPR), and False Positive Rate (FPR), are also considered.

The features extraction algorithms TSBTC, Otsu's thresholding, the machine learning algorithms and classifiers and feature fusion are further elaborated in the following subsections.

a. Thepade's Sorted Block Truncation Code (TSBTC) [8][9][10] **:**

Consider a histopathological image of size p x q and let R, G, and B represent red, green and blue planes, respectively. Each plane is then converted to a one-dimensional vector and sorted in increasing order. Each vector is divided into N distinct parts where N refers to the N-ary in Thepade SBTC N-ary. The feature vector comprises the centroid of each N part for the colour plane. So, in general, the feature vector will be composed of R_1, R_2, R_3, . . ., R_N, G_1, G_2, G_3, . . ., G_N, B_1, B_2, B_3, . . ., B_N. The general formula for calculating any R_i can be given as

$$R_i = \frac{N}{pq} \sum_{k=(i-1)\frac{pq}{N}}^{(i)\frac{pq}{N}} V_r\,[k] \tag{1}$$

Where V_r is the one-dimensional vector for the red plane sorted in increasing order, pq is the dimension of the image, and N represents the nth ary in Thepade SBTC n-ary. Similarly

$$B_i = \frac{N}{pq} \sum_{k=(i-1)\frac{pq}{N}}^{(i)\frac{pq}{N}} V_b\,[k] \tag{2}$$

$$G_i = \frac{N}{pq} \sum_{k=(i-1)\frac{pq}{N}}^{(i)\frac{pq}{N}} V_g\,[k] \tag{3}$$

Where V_b and V_g are the one-dimensional vectors sorted in increasing order for the blue and green planes, respectively

b. Otsu Thresholding Algorithm [11][12]:

Otsu's algorithm disregards the heterogeneity and variousness of the background, assuming the image comprises just the background and foreground(object). To address the issue of overlapping class distributions, the Otsu method employs a threshold to divide the image into two sections: P_0 (representing darker pixels) and P_1 (representing lighter pixels). P_0 is characterized by intensity levels ranging from 0 to t, denoted as P_0 = 0, 1, ..., t, while P_1 encompasses intensity levels from t to l-1, denoted as P_1 = t, t + 1, ..., l - 1, l. Here, t represents the threshold value, and l denotes the highest grey level of the image (e.g., 256). It is worth noting that P_0 and P_1 can be set to either foreground and background or vice versa, as the light region does not necessarily correspond to the object. This method involves an exhaustive examination of all possible threshold values to determine the optimal division between P_0 and P_1 based on the minimum pixel intensity values for each side of the threshold.

Given: For the observed grey value i=1, ..., l, the histogram probabilities are given as H(i)

$$H\,(i) = \frac{number\,\{(r,c)\ \mid image(r,c) = i\}}{(R,C)} \tag{4}$$

The column and row indices of the image are represented by c and r, respectively, while the number of columns and rows in the image are represented by C and R, respectively. The variance, mean, and weight of class T0 with intensity from 0 to t is given by $\sigma_b^2\,(t)$, $\mu_b\,(t)$, and $w_b\,(t)$, respectively.

The variance, mean, and weight of class T1 with intensity from t+1 to 1 are given $\sigma_f^2\,(t)$, $\mu_f\,(t)$, and $w_f\,(t)$, respectively.

σ_w^2 is the tallied average of the group variances. The value with the lowest within-class variance is the ideal threshold value, or t*. The within-class variance can be represented as follows:

$$\sigma_w^2\ = w_b\,(t) *\ \sigma_b^2\,(t)\ + w_f\,(t)\ * \sigma_f^2\,(t) \tag{5}$$

Where,

$$w\,(t) = \Sigma_{i=1}^{t}\ H\,(i) \tag{6}$$

$$w_f\,(t) = \Sigma_{i=t+1}^{l}\ H\,(i) \tag{7}$$

$$\mu_b\,(t) = \frac{\Sigma_{i=1}^{t}\ i * H\,(i)}{w_b\,(t)} \tag{8}$$

$$\mu_f(t) = \frac{\sum_{i=t+1}^{l} i * H(i)}{w_f(t)} \tag{9}$$

$$\sigma_b^2(t) = \frac{\sum_{i=1}^{t} (i - \mu_b(t))^2 * H(i)}{w_b(t)} \tag{10}$$

$$\sigma_f^2(t) = \frac{\sum_{i=t+1}^{t} (i - \mu_f(t))^2 * H(i)}{w_f(t)} \tag{11}$$

After obtaining t*, the input image $I(r, c)$ is segmented as

$$S(R, C) = \begin{cases} 1, & \text{if } I(r, c) > t* \\ 0, & \text{if } I(r, c) \leq t* \end{cases} \tag{12}$$

Utilizing the segmentation result $S(R, C)$, the intensity values of the input image $I(R, C)$ are partitioned into two clusters, facilitating the generation of the feature vector $[O1, O2]$, as delineated in equations 13 and 14.

$$O1 = \frac{1}{\sum_{i=1}^{r} \sum_{j=1}^{c} S(i, j)} \sum_{i=1}^{r} \sum_{j=1}^{c} I(i, j) * S(i, j) \tag{13}$$

$$O2 = \frac{1}{\sum_{i=1}^{r} \sum_{j=1}^{c} (1 - S(i, j))} \sum_{i=1}^{r} \sum_{j=1}^{c} I(i, j) * (1 - S(i, j)) \tag{14}$$

In this study, color images sourced from the KIMIA Path960 dataset are examined. The individual Red, Green, and Blue color channels of these images are isolated, yielding an Otsu Thresholding-based feature vector $[OR1, OR2, OG1, OG2, OB1, OB2]$ for each image in the dataset.

c. Feature Fusion of Thepade SBTC and Otsu Thresholding features of Histopathological images[13][14]:

The fusion of Thepade SBTC n-ary features and Otsu's thresholding is employed to achieve feature fusion for the classification of histopathological images. Considering a histopathological image with R, G and B representing the Red, Green, and Blue colour planes, respectively, the feature fusion vector combining Otsu's thresholding features and Thepade SBTC n-ary features can be denoted as [TR_1, TR_2, . . ., TR_n, TG_1, TG_2, . . ., TG_n, TB_1, TB_2, . . ., TB_n, OR_1, OR_2, OG_1, OG_2, OB_1, OB_2], where TR_i, TG_i and TB_i represent features of TSBTC n-ary while the rest represent features extracted using Otsu's Thresholding algorithm. Thus, it can be said that the feature vector will have the size 3n+6 where n is from TSBTC n-ary.

d. ML Classifiers and Algorithms Used:

Simple Logistics, Logistic Model Tree (LMT), KStar, Random Forest, Multilayer perceptron, IBK, Bayes' Net, Naive Bayes

e. Ensemble:

The ensemble is a machine learning methodology that involves amalgamating multiple base models to form a unified predictive model that aims to optimize predictive performance. Combining many models, an ensemble improves ML outcomes. Instead of using one single model, ensembles enable better prediction performance.

f. Majority Voting:

The majority voting technique integrates predictions from several machine learning models and ensembles to enhance model performance. By aggregating the results of different models, this method aims to produce superior outcomes compared to any single model used in the ensemble.

2.3 Experimentation Environment

The histopathological image classification method proposed is accomplished in Python with the help of Weka tool. The KIMIA Path960 dataset is considered for the entire experimentation. The dataset employed in this study comprises 400 images of various tissue types, including connective, muscle, and epithelial tissues. From these images, 20 scans representing distinct classes are selected, and 48 regions of interest of equal size are extracted from each whole slide image. These regions are then down-sampled to 308x168 patches for further analysis. Hence, a total of 960 (20x48) images are obtained. The images are saved as colour Tagged Image File (TFF) files. Figure **??** displays a subset of the images from the dataset.

The performance appraisal of all variations is done using percentage accuracy, Sensitivity, and Specificity. The values of these performances depend on False Positive, False Negative, True Positive, True Negative where,

TP - True Positive: When the histopathological picture is correctly identified, the outcome is a true positive.

FP - False Positive: When the histopathological picture is wrongly identified, the consequence is a false positive.

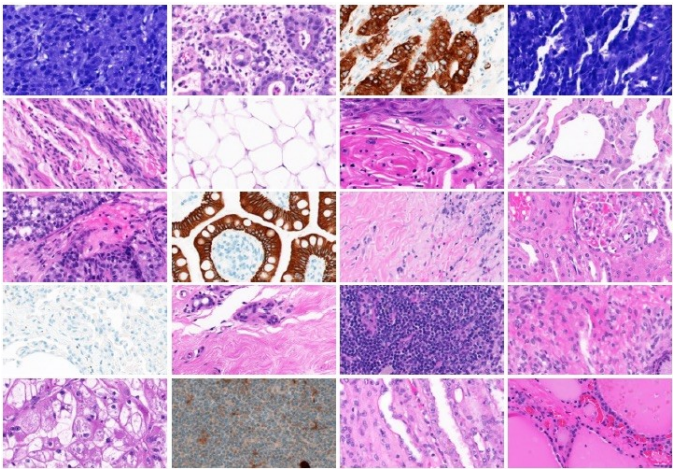

Figure 2: Samples from the KIMIA PATH960 dataset

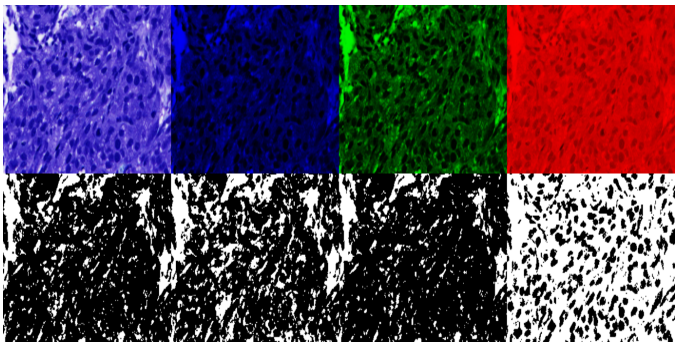

Figure 3: Binarized image of a sample from the dataset using Otsu's Thresholding Algorithm

TN - True Negative: It is an outcome in which the technique accurately detects the histopathological image that does not fit into the class of the image considered.

FN - False Negative: When a method mistakenly classifies a histopathological image as not in its original category, the result is a False Negative.

Then, the formulae for Specificity, Sensitivity, and accuracy can be given as follows:

$$Sensitivity = \frac{TP}{FN + TP} = TPRate \tag{15}$$

$$Accuracy = \frac{TP + TN}{TP + FP + FN + TN} \tag{16}$$

$$Specificity = \frac{TN}{TN + FP} = 1 - FPRate \tag{17}$$

3 Results and Discussions

The technique proposed experiments on 960 images of the KIMIA PATH960 dataset, where Thepade SBTC N-ary and Otsu thresholding algorithms are used for extracting global features. Twelve ML algorithms and eight ensembles are then used to train and test the features.

The percentage accuracy for histopathological image classification for TSBTC n-ary global features for twelve ML algorithms, namely SMO, Naive Bayes, Bayes' Net, Simple Logistics, Random Tree, Multilayer Perceptron, Random Forest, LMT, REPTree, KStar, IBK and J48 is shown in the table 1.

It can be inferred from Table 2 that the performance of Thepade SBTC bests Otsu's Thresholding for nearly all classifiers. The peak classification accuracy for the features extracted using TSBTC is 97.29% for TSBTC 7-ary with the LMT classifier, while the highest for Otsu's features was 94.48% with the LMT classifier. The graphical representation of the above data sheds further light on the performance of each feature extractor with individual classifiers. Figure **??** shows that for each classifier, the percentage accuracy for the features extracted using TSBTC n-ary increases from 2- ary to 7-ary and remains almost constant

Table 2: Percentage Accuracy for TSBTC N-ary and Otsu for different classifiers

Classifiers	2ary	3ary	4ary	5ary	6ary	7ary	8ary	9ary	10ary	Otsu
SMO	70.42	74.69	80.21	82.29	83.96	85.00	85.42	86.56	87.19	72.40
Bayes' Net	79.79	83.13	84.27	84.48	85.73	85.21	85.73	86.35	87.03	77.81
Naive Bayes	80.21	83.96	85.31	85.94	86.35	86.56	86.77	86.88	86.88	79.79
REPTree	81.46	82.81	83.96	86.25	86.04	85.42	86.98	85.83	87.64	81.56
LMT	93.54	95.94	96.46	96.56	96.25	97.29	96.56	96.88	96.67	94.48
SimpleLogistic	93.75	95.10	95.94	96.56	95.94	96.67	96.56	96.67	96.04	92.19
MultilayerPerceptron	93.33	93.65	95.21	95.63	95.10	95.31	95.21	95.94	96.35	88.75
RandomForest	90.63	91.77	93.13	94.06	94.17	94.27	94.48	95.79	94.48	88.44
KStar	90.31	92.19	92.60	93.54	93.85	94.38	94.27	94.27	94.48	88.44
lBk	90.21	91.25	92.71	93.13	93.02	93.23	93.23	93.23	93.54	89.48
J48	86.15	86.56	88.44	88.65	89.69	90.63	88.85	88.23	88.75	83.23
RandomTree	84.69	87.71	85.83	85.94	88.23	86.56	88.85	88.96	89.48	82.40

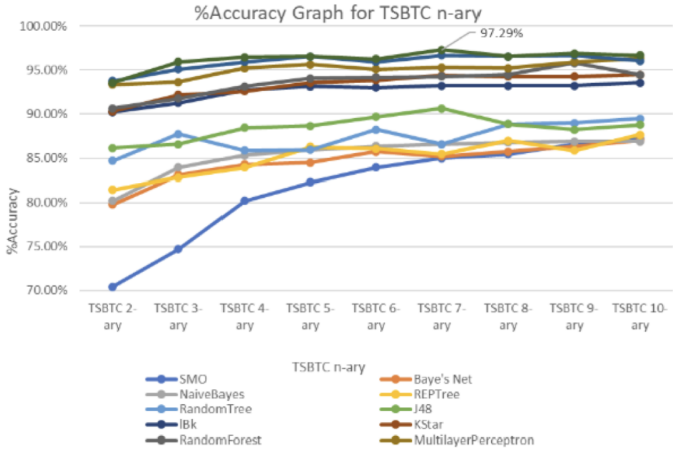

Figure 4: Performance Comparison of ML classifiers for Thepade SBTC n-ary

from 8-ary onwards. Also, it is worth noting that the classifiers KStar, RandomForest, Multilayer Perceptron, Simple Logistic and LMT gave better classification accuracies than the rest.

When the global features extracted from TSBTC and Otsu's Thresholding were fused, trained, and tested on the twelve classifiers, no performance amelioration was observed compared to TSBTC n-ary. The highest accuracy of 97.29% was obtained for the features of TSBTC 5-ary and Otsu with LMT classifier, which is the same for TSBTC 7-ary as observed before. Figure **??** shows a graphical representation of the same.

From Figure **??** and Figure **??**, it can be contemplated that the classifiers of KStar, Random Forest, Simple Logistic, Multilayer Perceptron, and Logistic Model Tree (LMT) performed better than the rest. Hence these classifiers are considered to form 8 distinct ensembles, namely – 'Logistic Model Tree+Simple Logistic+Multilayer Perceptron+Random Forest+KStar (LMT+SL+MP+RF+KS)', 'Simple Logistic+Multilayer Perceptron+Random Forest+Logistic Model Tree (SL+MP+RF+LMT)', 'Simple Logistic+Multilayer Perceptron+Random Forest (SL+MP+RF)', 'Simple Logistics+ Multilayer Perceptron+LMT (SL+MP+LMT)', 'Simple Logistic+Logistic Model Tree +Random Forest (SL + LMT + RF)', 'Simple Logistic+Logistic Model Tree (SL+LMT)', 'Simple Logistic+Multilayer Perceptron (SL+MP)', 'Random Forest+Simple Logistic (RF+SL).'

The extracted features are then trained and tested with the ensemble of classifiers to analyze performance improvement. Tables 3, 4 and 5 depict the result when ensembles are used to train and test the features extracted using TSBTC n-ary, Otsu and fusion of TSBTC and Otsu, respectively.

According to Table 3, the ensembles of LMT + Simple Logistics + Multilayer Perceptron + Random Forest + KStar and

Table 3: Performance (Accuracy) of Thepade SBTC n-ary for different ensembles

Classifiers	2ary	3ary	4ary	5ary	6ary	7ary	8ary	9ary	10ary
LMT + SL + MP + RF + KS	95.10	95.73	96.67	96.77	97.08	97.29	96.88	97.08	96.88
SL + MP + RF + LMT	95.10	96.15	96.98	96.77	96.98	97.29	97.08	97.08	96.98
SL + MP + RF	94.90	95.00	96.04	96.56	96.35	96.88	96.67	97.08	96.98
SL + MP	93.75	95.42	96.67	96.04	96.56	96.56	96.98	96.88	96.35
SL + RF	94.27	95.21	95.94	96.46	96.88	97.08	96.98	96.98	96.25
SL + RF + LMT	94.48	95.94	96.46	96.67	96.25	96.98	96.56	96.98	96.56
SL + LMT	93.85	96.04	96.56	96.67	96.46	97.08	96.56	96.98	96.46
SL + MP + LMT	94.79	95.94	96.77	96.56	96.25	97.19	96.56	96.88	96.67

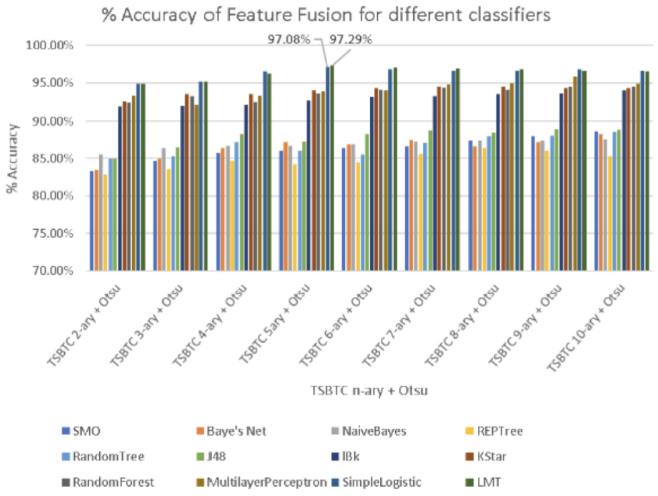

Figure 5: Performance Comparison of ML classifiers for the fusion of TSBTC n-ary + Otsu features

Table 4: Accuracy of Otsu for different ensembles

Classifiers	Otsu
LMT + SL + MP + RF + KS	92.3958
SL + MP + RF + LMT	93.8542
SL + MP + RF	91.8750
SL + RF + LMT	93.8542
SL + MP + LMT	93.9583
SL + MP	91.1458
SL + LMT	94.2708
SL + RF	93.0208

Simple Logistics + Multilayer Perceptron + Random Forest + LMT performed better for TSBTC 7-ary features, achieving an accuracy of 97.29%. Notably, the performance with ensemble learning was still the same as the highest accuracy achieved with the individual classifiers using Thepade SBTC n-ary features. From Tables 2 and 3, it can be concluded that Thepade SBTC 7-ary outperformed the other feature extractors with both individual classifiers and ensembles. A comparison of the best-performing Thepade SBTC 7-ary with the best-performing classifiers and ensembles is presented in Figure **??**. Although the ensemble of classifiers outperformed most individual classifiers, it is still evident from Figure **??** that further improvement is required to achieve the highest accuracy.

Ensemble learning was ineffective for the features extracted using Otsu's Thresholding, as the performance did not improve when an ensemble of classifiers was used. The highest accuracy obtained in this case was 94.27% for the Simple Logistic and LMT classifiers ensemble, which was lower than the 94.48% accuracy achieved by the LMT classifier alone, as shown in Table 2.

Nevertheless, the application of ensemble learning demonstrated notable success when combining Thepade SBTC and Otsu

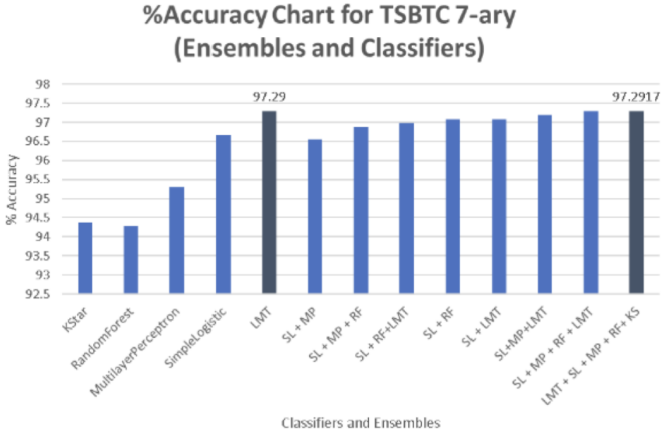

Figure 6: Performance comparison of ML classifiers and ensemble of classifiers for TSBTC 7-ary

Table 5: Performance (Accuracy) of TSBTC n-ary with various ensemble of classifiers

Classifiers	2ary	3ary	4ary	5ary	6ary	7ary	8ary	9ary	10ary
LMT + SL + MP + RF + KS	95.83	95.73	96.56	96.77	96.46	97.29	96.77	96.77	96.67
SL + MP + RF + LMT	96.15	95.83	96.67	97.08	97.08	97.29	96.77	96.98	96.35
SL + MP + RF	95.21	95.10	96.15	96.15	96.04	96.88	96.46	96.56	96.04
SL + MP	95.10	95.31	96.25	96.25	96.56	97.08	96.67	96.56	96.35
SL + RF	95.63	95.31	96.46	96.56	96.88	97.08	96.77	96.77	96.77
SL + RF + LMT	95.63	95.83	96.88	97.19	96.88	97.39	96.67	96.77	96.67
SL + LMT	95.31	95.31	96.56	97.08	96.98	97.29	96.67	96.56	96.67
SL + MP + LMT	95.52	95.94	96.88	97.08	97.08	97.39	96.67	96.98	96.67

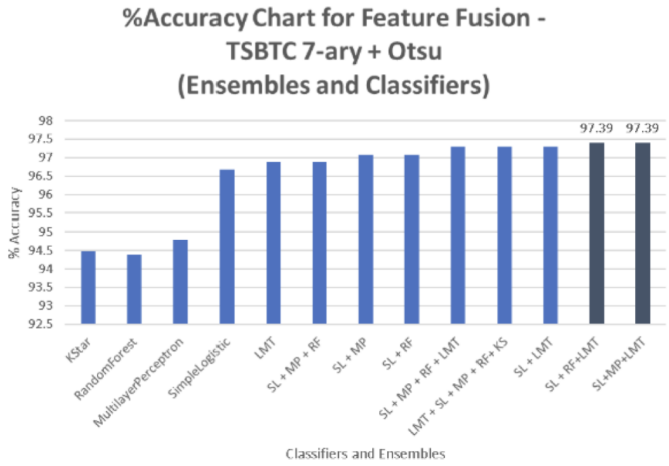

Figure 7: Performance comparison of ML classifiers and ensemble of classifiers

features. From the results in Table 3, it can be observed that for feature fusion, better performance was obtained with ensembles of Simple Logistic, Multilayer Perceptron, and Logistics Model Tree, as well as with ensembles of Simple Logistic, Random Forest, and LMT classifiers. These ensembles achieved an accuracy of 97.39%, which outperformed the accuracy obtained with the LMT classifier alone for the same features. A comparison chart of the classification accuracy for 7-ary + Otsu with the best classifiers and ensembles is shown in Figure **??**.

While ensemble learning did not yield significant improvements for features extracted by TSBTC or Otsu, it did demonstrate performance improvements for a fusion of the features extracted through these techniques. It is important to note that the fusion of features obtained through Otsu and TSBTC 7-ary with the aforementioned ensembles achieved the best overall performance compared to all other feature extraction techniques described in the research.

From all the graphs and tables, it can be implied that among TSBTC n-ary features, the features extracted by TSBTC 7-ary performed better than the rest when tested with both individual as well as ensemble of classifiers. Though global features were extracted using TSBTC and Otsu, the features extracted using TSBTC performed better than that of Otsu. When the global features extracted through the aforementioned algorithms were combined, the feature fusion performed better than the rest of the ensemble of classifiers. Though 5-ary + Otsu features with LMT classifier performed better than the rest with individual classifiers, an ensemble of classifiers with feature fusion of TSBTC 7-ary + Otsu bettered it. A comparison of 7-ary, Otsu and 7-ary + Otsu features for different ensembles and best classifiers is shown in figure **??**.

Performance metrics like specificity, sensitivity and f-measure were also considered to investigate the performance further. A graphical plot of the same is shown in Figure **??**.

The feature fusion exhibited the highest precision, Recall, sensitivity, and specificity values, as observed in Figure **??**. In comparison, using individual features of Thepade SBTC 7-ary or Otsu yielded lower values. The chart further reinforces the notion that feature fusion does help in the classification of histopathological images.

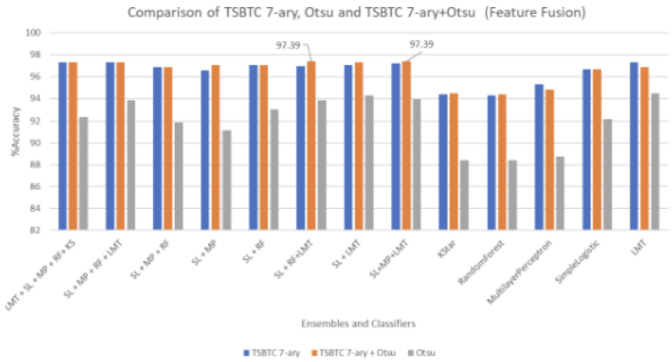

Figure 8: Comparison of TSBTC 7-ary, Otsu and TSBTC 7-ary + Otsu (feature fusion)

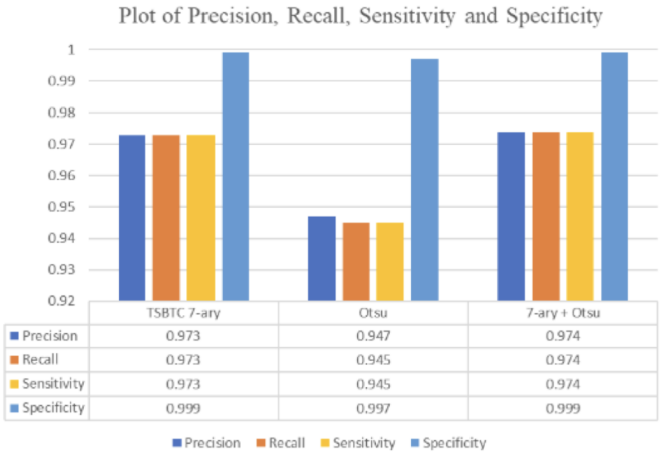

Figure 9: Plot of precision, recall, sensitivity and specificity for TSBTC 7-ary, Otsu and TSBTC 7-ary + Otsu

Table 6: Comparison of all related work on KIMIA path 960 dataset

Authors	Methodology	Dataset	Technique employed	Performance metrics	
Meghna et al. [1]	LBP, BoVW, CNN	KIMIA Path960	BoVW	Accuracy	96.50%
			LBP	Accuracy	90.62%
			Deep features	Accuracy	94.72%
Taha et al. [2]	Deep Features, HOG and LBP	KIMIA Path960	SVM + LBP feature	Accuracy	90.52%
			SVM + deep features	Accuracy	81.14%
			ANN + HOG	Accuracy	34.37%
Ganguly et al. [3]	Optimization Algorithms in Combination with Deep Learning Models	KIMIA Path960	ResNet50 + Radam	Accuracy	99.27%
			ResNet50 + AdaMax	Accuracy	99.79%
			ResNet50 + Adam	Accuracy	99.77%
			ResNet50 + AdamW	Accuracy	99.90%
Anish et al. [4]	Feature Blending	KIMIA Path960	Sorted gray value Mean + GLCM + NN	Recall	0.951
				Precision	0.951
				F1 score	0.951
				AUC	0.999
			Sorted gray value Mean + GLCM + RF	Recall	0.926
				Precision	0.927
				F1 score	0.926
				AUC	0.997
			Sorted gray value Mean+ GLCM + SVM	Recall	0.917
				Precision	0.919
				F1 score	0.916
				AUC	0.998
Proposed Method	Fusion of TSBTC and Otsu features	KIMIA Path960	Ensemble of SL + MP + LMT with TSBTC 7-ary Otsu features	Specificity	0.999
				Sensitivity	0.974
				Accuracy	97.39%
			Ensemble with Thepade SBTC 7-ary features	Specificity	0.999
				Sensitivity	0.973
				Accuracy	97.29%
			LMT with Otsu features	Specificity	0.997
				Sensitivity	0.947
				Accuracy	94.70%

4 Conclusions

Feature extraction is a crucial step in the classification of histopathological images. Literature has given several feature extraction techniques. This paper proposes Thepade SBTC and Otsu Binarization techniques for feature extraction. The fusion of these features is also considered to enhance the classification accuracy of histopathological images. Also, in an attempt to create a more robust model for accurate prediction, ensembles of classifiers were considered. It was observed from the experimentation that almost all classifiers and ensemble combinations gave better performance for the global features extracted using Thepade SBTC in comparison to Otsu. The classification accuracy was improved when the features were combined, and the resultant features were trained and tested using ensemble of classifiers. Better performance is observed by ensembles of Simple Logistics, Multilayer Perceptron, Logistics Model Tree and also Simple Logistics, Random Forest, and LMT classifiers for the fusion of TSBTC 7ary and Otsu features with an accuracy of 97.39% in 10-fold cross-validation scenario. The results emphasize the optimality of feature fusion and ensemble learning in the classification of histopathological images. Additionally, the application of this method to classify histopathological images, particularly in the context of diseases like cancer, presents an exciting opportunity for future investigations.

5 Authors' Contributions

Sudeep T. contributed to the ideation phase, conceptualizing the research framework and generating initial ideas. Implementation, experimental explorations, analysis, and drafting were all equally contributed by both authors, Sudeep T. and Ashwin A. Both authors equally invested in the integrity and quality of the research presented.

6 Competing Interests

The authors declare that they have no competing interests.

References

[1] M Dinesh Kumar, M Babaie, S Zhu, S Kalra, and HR Tizhoosh. A comparative study of cnn, bovw and lbp for classification of histopathological images. In *IEEE Symposium Series on Computational Intelligence (SSCI)*, pages 1–7, 2017.

[2] TJ Alhindi, S Kalra, KH Ng, A Afrin, and HR Tizhoosh. Comparing lbp, hog and deep features for classification of histopathology images. In *International Joint Conference on Neural Networks (IJCNN)*, pages 1–7, 2018.

[3] A Ganguly, R Das, and SK Setua. Histopathological and lymphoma image classification using customized deep learning models and optimization algorithms. In *11th International Conference on Computing, Communication and Networking Technologies (ICCCNT)*, pages 1–7, 2020.

[4] A Anurag, R Das, GK Jha, SD Thepade, N D'Souza, and C Singh. Feature blending approach for efficient categorization of histopathological images for cancer detection. In *IEEE Pune Section International Conference (PuneCon)*, pages 1–6, 2021.

[5] RR Kadhim and MY Kamil. Evaluation of machine learning models for breast cancer diagnosis via histogram of oriented gradients method and histopathology images. *International Journal on Recent and Innovation Trends in Computing and Communication*, (10), 2022.

[6] I Hirra, M Ahmad, A Hussain, MU Ashraf, IA Saeed, SF Qadri, AM Alghamdi, and AS Alfakeeh. Breast cancer classification from histopathological images using patch-based deep learning modelling. *IEEE Access*, 9:24273–24287, 2021.

[7] R Rashmi, K Prasad, and CBK Udupa. Bchisto-net: Breast histopathological image classification by global and local feature aggregation. *Artificial Intelligence in Medicine*, 121:102191, 2021.

[8] S Khairnar, SD Thepade, and S Gite. Effect of image binarization thresholds on breast cancer identification in mammography images using otsu, niblack, burnsen, thepade's sbtc. *Intelligent Systems with Applications*, 2021.

[9] SD Thepade and Y Bafna. Improving the performance of machine learning classifiers for image category identification using feature level fusion of otsu segmentation augmented with thepade's n-ary sorted block truncation coding. In *2018 Fourth International Conference on Computing Communication Control and Automation (ICCUBEA)*, pages 1–6, 2018.

[10] S. D. Thepade and P. R. Chaudhari. Land usage identification with fusion of thepade sbtc and sauvola thresholding features of aerial images using ensemble of machine learning algorithms. *Applied Artificial Intelligence*, 35:154–170, 2020.

[11] N Otsu. A threshold selection method from gray-level histograms. *IEEE Transactions on Systems, Man, and Cybernetics*, 9(1):62–66, 1979.

[12] J Yousefi. Image binarization using otsu thresholding algorithm. 2015.

[13] P Rahim, N Mustafa, H Yazid, TX Jian, S Daud, and K Rahman. Segmentation of tumour region on breast histopathology images to assess glandular formation in breast cancer grading. *Journal of Physics: Conference Series*, 2071:012051, 2021.

[14] MK Slifka and JL Whitton. Clinical implications of dysregulated cytokine production. *J. Mol. Med.*, 78:74–80, 2000.